

光学学报

数字光弹性中六步混合相移技术

邱川¹, 陈念年¹, 巫玲^{1*}, 范勇^{1**}, 刘光海²

¹西南科技大学计算机科学与技术学院, 四川 绵阳 621010;

²四川物科光学精密机械有限公司, 四川 绵阳 621010

摘要 数字光弹性应力分析中常用相移法确定等倾线和等差线,最广泛应用的是十步相移法,针对单色光入射引起的等倾线耦合等差线的问题,增加采集白光入射 4 幅图像,使用不同光弹图像集分别计算等倾线和等差线,测量精度更高但操作复杂、效率较低。本文提出一种优化的六步混合相移方法,将十步相移法的 6+4 测量方法缩减为 3+3 的六步测量方法。用仿真模拟实验对本文方法进行误差分析,验证了其具有良好的抗噪性能和相移误差抗干扰能力。真实实验结果表明:与传统六步相移法相比,本文方法有效解决了等倾线耦合等差线以及波片失配误差的问题;与十步相移法相比,本文方法与其等倾线平均偏差约为 0.01 rad,等差线平均偏差约为 0.09 rad,在提高 40% 采集效率的同时保证了测量精度。

关键词 物理光学; 数字光弹性; 相移法; 等倾线; 等差线

中图分类号 O348.1

文献标志码 A

DOI: 10.3788/AOS221978

1 引言

数字光弹性技术是一种实验力学分析的光学技术^[1-2],它能直观地以条纹图的形式给出应力场相关信息,即主应力方向角的等倾线和主应力差的等差线。等差线和等倾线可以用单幅光弹性图像和多幅光弹性图像进行计算。采用单幅图像分析的傅里叶变换方法^[3]存在难以同时计算等差线和等倾线的不足,其计算成本较高,应用较少^[4]。采用相移技术^[5-8]的多幅光弹图像分析法因其计算简单、准确而被广泛应用于牙医学、生物学、断裂力学等领域的应力分析中。

Patterson 等^[9]于 1991 年提出了六步相移法,该方法计算出的等倾线存在耦合等差线的问题^[10-12]。1998 年,文献[13]提出改进的六步相移法,采用左右旋圆偏振光采集图像,降低了四分之一波片失配误差。1990 年,文献[14]提出用平面偏振光场的四步相移计算等倾线。上述相移法均采用单色光,其等差线在整数级和半整数级区域会发生消光现象,等倾线也被此噪声干扰,出现不连续锯齿显现。1997 年,文献[15]采用白光光源替换单色光源,由于不同波长的等差线整数级和半整数级区域不同,因此不会出现局部的等差线干扰等倾线的问题。2003 年,文献[16]提出确定等倾线的光弹性五步彩色相移法,为了减少测量误差,在相移法中引入背景光强。2006 年,文献[17]对各种方法进行比较,得出平面偏振光场采集的光弹图像更适合

计算等倾线;2008 年进一步提出组合四步相移法和六步相移法的十步相移技术^[18],该方法成为了目前光弹性应力分析中一种最常用的方法^[19-20],但也存在需要采集与计算的光弹图像较多、实验采集效率较慢的问题。2014 年,文献[21]提出了一种二维双折射测量系统,该系统添加了偏振图像传感器,一次能采集多幅光弹图像。2020 年,文献[22]采用高速偏振相机一次性采集 4 幅光弹图像,可用于计算等倾线和等差线,但是仍然没有克服等倾线耦合等差线的问题。2022 年,文献[23]使用偏振相机采集图像,分别旋转 4 次光学元件,采集 16 幅光弹图像实现十步相移法。以上方法都是通过改进采集装置来间接提高图像采集效率,但所需偏振相机价格昂贵。

本文分析了十步相移理论公式,提出了满足平面偏振光场中计算等倾线和圆偏振光场中计算等差线这两个要求的最简相移方案,以实现测量精度和效率的平衡。通过对径向受压圆盘进行的应力实验,证明了该方法的正确性与可行性。

2 六步相移和十步相移的原理及问题

图 1(a)为平面偏振光学系统,光源(S)和沿光源(S)轴线方向上依次设置的起偏镜(P)、载荷装置(M)、检偏镜(A)。图 1(b)为圆偏振光学系统,光源(S)和沿光源(S)轴线方向上依次设置的起偏镜(P)、第一四分之一波片(Q1)、载荷装置(M)、第二四分之

收稿日期: 2022-11-14; 修回日期: 2022-12-17; 录用日期: 2023-01-16; 网络首发日期: 2023-02-07

基金项目: 四川省省级科研院所科技成果转化项目(22YSZH0021)、四川省科技厅重点研发项目(2021YFG0031)

通信作者: *wuling751@126.com; **419595203@qq.com

一波片(Q2)、检偏镜(A)。六步相移在图1(b)圆偏振光学系统下,对应不同的偏振场设置以及不同的光强

等式,如表1所示。

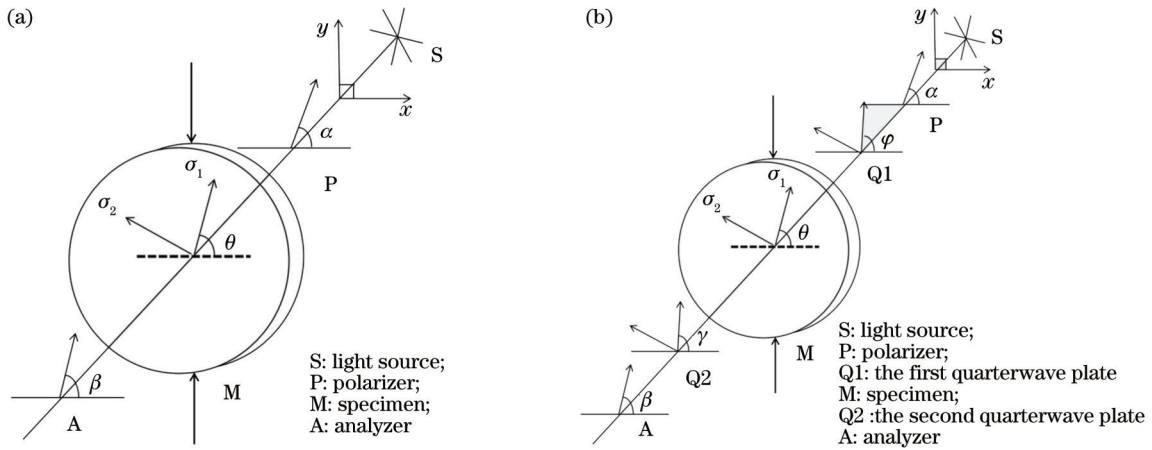


图1 偏振光学系统。(a)平面偏振光学系统;(b)圆偏振光学系统

Fig. 1 Polarization optical system. (a) Planar polarization optical system; (b) circular polarization optical system

表1 六步相移的光强方程

Table 1 Intensity equations of six-step phase shift

Number	α	φ	γ	β	Intensity
I_1	$\pi/2$	$\pi/4$	$-\pi/4$	0	$I_1 = I_b + \frac{I_c}{2}(1 - \cos \delta)$
I_2	$\pi/2$	$\pi/4$	$-\pi/4$	$\pi/2$	$I_2 = I_b + \frac{I_c}{2}(1 + \cos \delta)$
I_3	$\pi/2$	$\pi/4$	0	$\pi/2$	$I_3 = I_b + \frac{I_c}{2}(1 - \sin \delta \sin 2\theta)$
I_4	$\pi/2$	$\pi/4$	$\pi/4$	$3\pi/4$	$I_4 = I_b + \frac{I_c}{2}(1 + \sin \delta \cos 2\theta)$
I_5	$\pi/2$	$\pi/4$	0	0	$I_5 = I_b + \frac{I_c}{2}(1 + \sin \delta \sin 2\theta)$
I_6	$\pi/2$	$\pi/4$	$\pi/4$	$\pi/4$	$I_6 = I_b + \frac{I_c}{2}(1 - \sin \delta \cos 2\theta)$

表1中 I_b 为背景光强, I_c 为单色光的光源光强, θ 表示为第一主应力方向角, δ 表示通过应力模型产生的相位差。则六步相移计算等倾线 θ 和等差线 δ 公式分别为

$$\theta = \frac{1}{2} \arctan \left(\frac{I_3 - I_5}{I_6 - I_4} \right) = \frac{1}{2} \arctan \left(\frac{I_c \sin \delta \sin 2\theta}{I_c \sin \delta \cos 2\theta} \right), \sin \delta \neq 0, \quad (1)$$

$$\delta = \arctan \left[\frac{(I_5 - I_3) \sin 2\theta_u + (I_4 - I_6) \cos 2\theta_u}{I_2 - I_1} \right], \quad (2)$$

式中: θ_u 表示去包裹后的等倾线相位。由式(1)得到全场范围内 $[-\pi/4, \pi/4]$ 等倾线包裹相位图, 去包裹得到 $[-\pi/2, \pi/2]$ 范围的等倾线 θ_u 。

图2(a)和(b)的红色框中出现等倾线耦合等差线问题, 即等倾线受等差线干扰, 出现了不连续的锯齿形缺陷。原因是所用单色光源的等倾线在等差线的整数

级和半整数级区域会发生消光现象。白光则是由不同波长光组成, 不同光的整数级区域位于不同的位置, 不会出现同时消光, 因此图2(c)的等倾线没有出现局部等差线干扰的问题。

十步相移法计算等差线的方法与六步相移法相同, 因此修改了计算等倾线的方法, 将式(1)调整为

$$\theta = \frac{1}{4} \arctan \left(\frac{\tilde{I}_{w4} - \tilde{I}_{w2}}{\tilde{I}_{w3} - \tilde{I}_{w1}} \right) = \frac{1}{4} \arctan \left(\frac{I_s \sin^2 \frac{\delta}{2} \sin 4\theta}{I_s \sin^2 \frac{\delta}{2} \cos 4\theta} \right), \sin \frac{\delta}{2} \neq 0, \quad (3)$$

式中: I_s 是白光的光源光强; \tilde{I}_w 表示图像 R、G、B 三通道的平均值, 得到 $[-\pi/8, \pi/8]$ 的等倾线 θ 。其对应不同的偏振场设置以及不同的光强等式如表2所示。

由表2和式(3)可知, 相比于六步相移, 十步相移增加了白光入射的4幅图像, 导致需要采集光弹性条

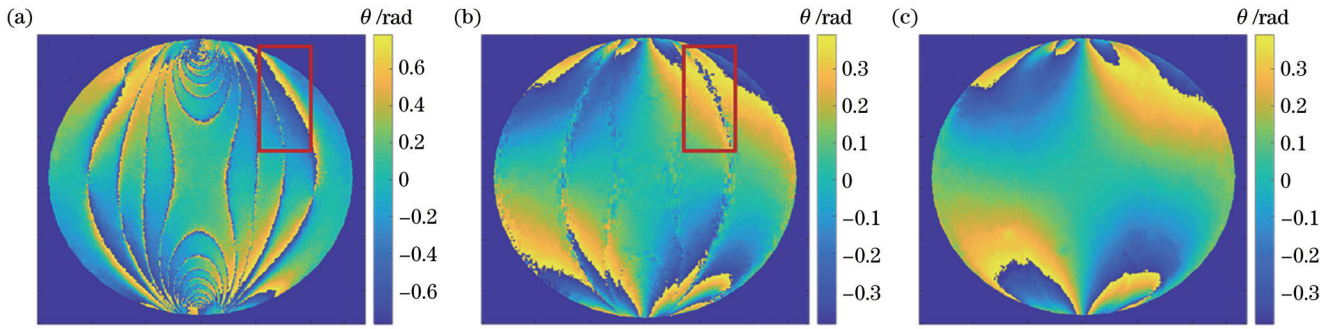


图 2 等倾线图像。(a)单色光的六步相移;(b)单色光的十步相移;(c)白光的十步相移

Fig. 2 Isoclinic images. (a) Six-step phase shift with monochromatic light; (b) ten-step phase shift with monochromatic light; (c) ten-step phase shift with white light

表 2 四步相移技术的光强方程

Number	α	β	Intensity
I_{w1}	$\pi/2$	0	$I_{w1} = I_b + I_s \sin^2 \frac{\delta}{2} \sin^2 2\theta$
I_{w2}	$5\pi/8$	$\pi/8$	$I_{w2} = I_b + \frac{I_s}{2} \sin^2 \frac{\delta}{2} (1 - \sin 4\theta)$
I_{w3}	$3\pi/4$	$\pi/4$	$I_{w3} = I_b + I_s \sin^2 \frac{\delta}{2} \cos^2 2\theta$
I_{w4}	$7\pi/8$	$3\pi/8$	$I_{w4} = I_b + \frac{I_s}{2} \sin^2 \frac{\delta}{2} (1 + \sin 4\theta)$

表 3 平面偏振光场的三幅图像

One image	Two images	
	I_{w1} and I_{w3}	I_{w2} and I_{w4}
I_{w1}	0	1
I_{w2}	1	0
I_{w3}	0	1
I_{w4}	1	0

Notes: 1 represents three images that can be combined, 0 represents three images that cannot be combined.

纹图像较多,采集效率更低。

3 六步混合相移法

考虑到六步相移和十步相移各自的不足,本文提出一种的六步混合相移法,既能实现六幅光弹图像计算等倾线和等差线,又能避免等倾线耦合等差线的问题。根据表 2,为了求解 I_b 、 I_s 、等倾线 θ 三个未知量,采用了 $I_{w1} \sim I_{w4}$ 四个光强等式。其关系为

$$I_{w1} + I_{w3} = I_{w2} + I_{w4} = 2I_b + I_s \sin^2(\delta/2), \quad (4)$$

式中: I_{w1} 与 I_{w3} 、 I_{w2} 与 I_{w4} 相互补偿。例如,可以将 I_{w4} 光强等式变换为

$$I_{w4} = (I_{w1} + I_{w3}) - I_{w2}, \quad (5)$$

式中: I_{w4} 就可以用 I_{w1} 、 I_{w2} 、 I_{w3} 进行表示。因此,我们只需要用白光作为光源,平面偏振光场采集三幅图像便可以计算等倾线 θ ,但这样的三幅图像有多种组合形式,如表 3 所示。

表 3 中 1 表示可以组合的三幅图像,0 表示不能组合的三幅图像。例如,选择表 3 中的 I_{w1} 、 I_{w2} 、 I_{w3} 组合成三步相移,则计算等倾线 θ 公式为

$$\theta = \frac{1}{4} \arctan \left(\frac{\tilde{I}_{w3} + \tilde{I}_{w1} - 2\tilde{I}_{w2}}{\tilde{I}_{w3} - \tilde{I}_{w1}} \right), \sin \frac{\delta}{2} \neq 0. \quad (6)$$

同理,根据表 1,为了求解 I_b 、 I_c 、等差线 δ 三个未知量,采用了六步相移法中 $I_1 \sim I_6$ 的 6 个光强等式。其关系式为

$$I_1 + I_2 = I_5 + I_3 = I_4 + I_6 = 2I_b + I_c. \quad (7)$$

根据式(7)可知, I_1 与 I_2 、 I_5 与 I_3 以及 I_4 与 I_6 相互补偿。在式(6)等倾线已计算的条件下,为了减少参与运算的图像数量,可以实现用单色光作光源,圆偏振光场采集三幅图像求解以上三个未知量。例如,选择表 1 中 I_1 、 I_2 、 I_6 的组合方式,则计算等差线 δ 公式为

$$\delta = \arctan \frac{I_1 + I_2 - 2I_6}{(I_2 - I_1) \cos 2\theta_u} = \arctan \frac{I_c \sin \delta \cos 2\theta_u}{I_c \cos \delta \cos 2\theta_u}. \quad (8)$$

这样的三幅图像同样有多种组合形式,如表 4 所示。

综上,本文采用白光入射的平面偏振光场获取三幅彩色光弹图像计算等倾线、单色光入射圆偏振光场

表 4 圆偏振光场的三幅图像

One image	Two images		
	I_1 and I_2	I_3 and I_5	I_4 and I_6
I_1	0	1	1
I_2	0	1	1
I_3	1	0	0
I_4	1	0	0
I_5	1	0	0
I_6	1	0	0

Notes: 1 represents three images that can be combined, 0 represents three images that cannot be combined.

获取三幅单色光弹图像计算等差线的混合相移方法,既解决了传统六步相移法中等倾线耦合等差线的问题,又提高了目前广泛使用的十步相移法的效率。

从理论分析可以看出,本文方法可以采用更少的图像等效十步相移法的等倾线和等差线计算,平衡精度和效率。

4 实验及结果分析

4.1 实验平台与方案

实验采用聚碳酸酯材料的径向压缩圆盘,圆盘直径 $D=50\text{ mm}$,厚度 $h=4\text{ mm}$,重复实验改变载荷、材料尺寸等条件,每次实验采集表 1 和表 2 中所有 10 张光弹图像。实验装置如图 3 所示。

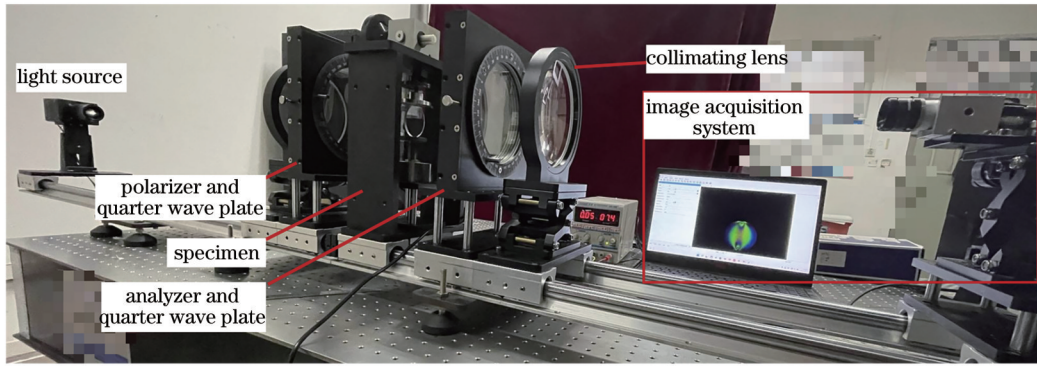


图 3 数字光弹性图像采集系统

Fig. 3 Digital photoelastic image acquisition system

表 5 各方法加噪前后的等倾线和等差线平均偏差结果

Table 5 Average deviation results of isoclinic and isochromatic before and after noise of each method

Images SNR /dB	Deviation results of isoclinic B / rad		Deviation results of isochromatic B / rad	
	Proposed method	Ten-step phase shift	Proposed method	Ten-step phase shift
40	0.0173	0.0141	0.0286	0.0199
45	0.0097	0.0098	0.0170	0.0120
50	0.0058	0.0046	0.0098	0.0079

从表 5 的实验结果可以看出,本文方法在不同噪声水平下计算的等倾线和等差线偏差总体与十步相移法相当,表明其有良好的抗噪性能,而部分偏差十步相移法相对更小,其原因是十步相移采集的图片更多,抗噪性能总体更强。

4.2 算法误差分析实验

4.2.1 算法抗噪性能分析

考虑到 CCD 成像过程中引入了高斯白噪声,对径向压缩圆盘进行仿真的图像加入不同等级的高斯噪声,以验证本文方法的抗噪性能。然后,采用十步相移法和本文方法分别计算等倾线和等差线相位图,进一步计算加噪前后的等倾线和等差线偏差。

$$B = \frac{\sum_{i \in \Omega} |X_i - x_i|}{\sum_{i \in \Omega} 1}, \quad (9)$$

式中: Ω 表示光弹图像有效区域;下标 i 表示像素数量; X 表示各方法加噪后计算的图像; x 表示各方法加噪前计算的图像。在不同载荷下,分别重复 10 次实验,等倾线和等差线的平均偏差结果如表 5 所示。

4.2.2 方位角误差分析

在光弹实验中,需要旋转起偏镜、四分之一波片、检偏镜等光学器件采集图像,不可避免地会造成方位角误差,从而引起相移误差。假设含方位角误差的平面偏振光场光强公式为

$$I_w = I_b + I_a \left\{ \cos^2 [(\beta \pm \Delta\beta) - (\alpha \pm \Delta\alpha)] \cos^2 (\delta/2) + \cos^2 [(\beta \pm \Delta\beta) + (\alpha \pm \Delta\alpha) - 2\theta] \sin^2 (\delta/2) \right\}, \quad (10)$$

式中: β 为检偏镜理论旋转的角度; α 为起偏镜理论旋转的角度; $\Delta\beta$ 则为检偏镜方位角偏差值; $\Delta\alpha$ 为起偏镜方位角偏差值。同理,含方位角误差的圆偏振光场光强公式为

$$I = I_b + \frac{I_c}{2} \left\{ 1 - \sin 2 [(\beta \pm \Delta\beta) - (\gamma \pm \Delta\gamma)] \cos \delta + \sin 2 [\theta - (\gamma \pm \Delta\gamma)] \cos 2 [(\beta \pm \Delta\beta) - (\gamma \pm \Delta\gamma)] \sin \delta \right\}, \quad (11)$$

式中: γ 为波片理论旋转角度; $\Delta\gamma$ 为波片方位角偏差; θ 是第一主应力与水平 x 轴的夹角; δ 是光通过应力模型

产生的相位差。采用式(10)和式(11)仿真模拟生成含各方位角偏差的对径向压缩圆盘图像。采用本文方法

和十步相移法分别处理这些图像,计算等倾线和等差线,并采用式(9)计算等倾线和等差线平均偏差,以验证本文方法对相移误差的抗干扰性能。具体实验结果如表 6、7 所示,其中, $\Delta\beta$ 和 $\Delta\alpha$ 、 $\Delta\gamma$ 和 $\Delta\beta$ 偏差有多种组合情况。

表 6 起偏镜、检偏镜的方位角引起等倾线的偏差结果
Table 6 Deviation results of isoclinic caused by azimuth of polarizer and analyzer

Azimuth deviation	Deviation of isoclinic B /rad	
	Proposed method	Ten-step phase shift
$\Delta\alpha=0.4^\circ, \Delta\beta=0.4^\circ$	0.0127	0.0127
$\Delta\alpha=-0.4^\circ, \Delta\beta=-0.4^\circ$	0.0127	0.0127
$\Delta\alpha=-0.4^\circ, \Delta\beta=0.4^\circ$	1.318×10^{-13}	1.318×10^{-13}
$\Delta\alpha=0^\circ, \Delta\beta=0.4^\circ$	0.0064	0.0064
$\Delta\alpha=0.4^\circ, \Delta\beta=0^\circ$	0.0064	0.0064

从表 6 的实验结果可以看出,本文方法在不同方位角误差下计算的等倾线偏差与十步相移一致,表明本文方法与十步相移法具有相同的抗相位误差干扰能力。从表 7 的实验结果可以看出,本文方法在不同方

表 7 第二四分之一波片、检偏镜方位角引起等差线的偏差结果

Table 7 Deviation results of isochromatic caused by the azimuth of the second quarter wave and the analysis mirror

Azimuth deviation	Deviation of isochromatic B /rad	
	Proposed method	Ten-step phase shift
$\Delta\gamma=0.4^\circ, \Delta\beta=0.4^\circ$	6.647×10^{-17}	4.664×10^{-17}
$\Delta\gamma=-0.4^\circ, \Delta\beta=0.4^\circ$	0.0322	0.0171
$\Delta\gamma=0^\circ, \Delta\beta=0.4^\circ$	0.0160	0.0085
$\Delta\gamma=0.4^\circ, \Delta\beta=0^\circ$	0.0159	0.0085
$\Delta\gamma=-0.4^\circ, \Delta\beta=0^\circ$	0.0170	0.0085

位角误差下计算的等差线偏差均近似两倍于十步相移法,其原因在于十步相移法使用六幅图像计算等差线,而本文方法只需要三幅图像,一定程度上损失了部分有效信息,故抗相位误差干扰能力相对十步相移法弱。从表 6、7 还可以看出,实际应用中应尽量减少方位角误差,可以获得精度更高的等倾线和等差线计算结果。

4.3 等倾线实验结果分析

图 4 是分别改变载荷 F 和圆盘直径 D 条件下,各种相移方法计算出的等倾线。

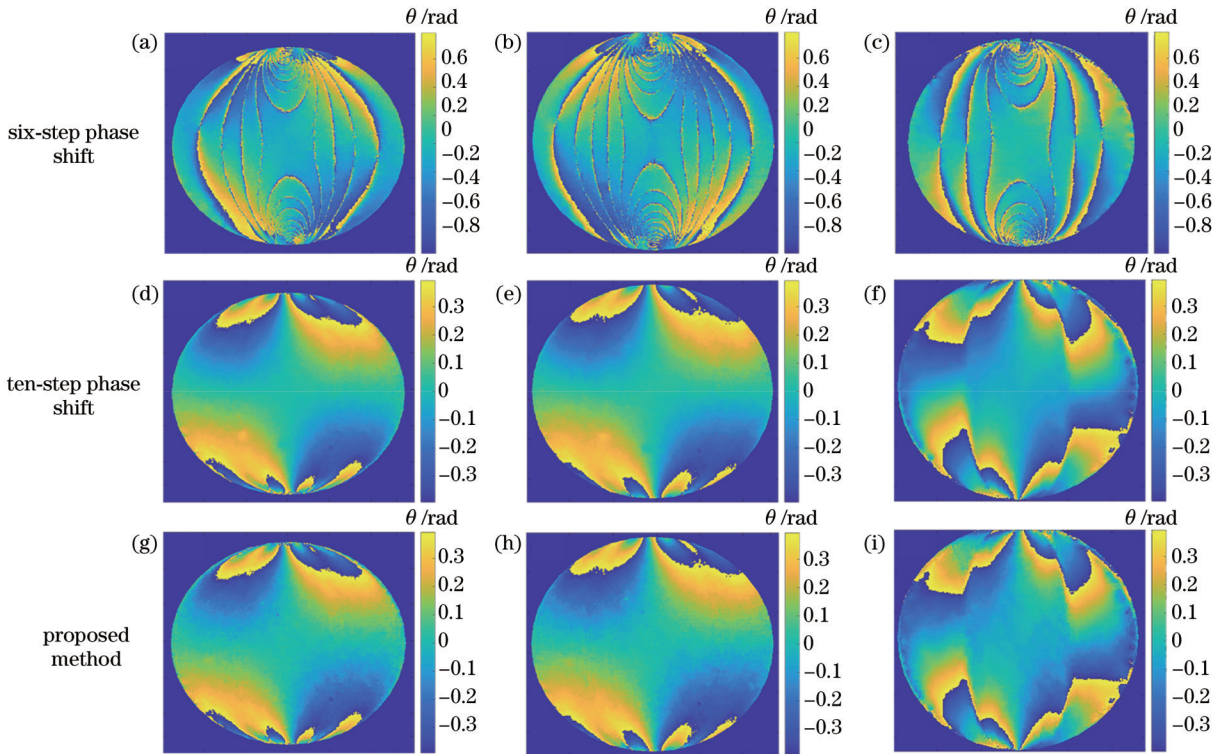


图 4 包裹的等倾线图像。(a)(d)(g) $F=200\text{ N}$, $D=50\text{ mm}$; (b)(e)(h) $F=350\text{ N}$, $D=50\text{ mm}$; (c)(f)(i) $F=200\text{ N}$, $D=40\text{ mm}$
Fig. 4 Wrapped isoclinic images. (a)(d)(g) $F=200\text{ N}$, $D=50\text{ mm}$; (b)(e)(h) $F=350\text{ N}$, $D=50\text{ mm}$; (c)(f)(i) $F=200\text{ N}$, $D=40\text{ mm}$

图 4(a)(d)(g)与(b)(e)(h)是不同载荷下对比,图 4(a)(d)(g)与(c)(f)(i)是不同圆盘直径下对比。从图 4 可以直观看出,本文方法与十步相移的等倾线图像一致。传统六步相移法的等倾线受等差线噪声干扰,这会其去包裹结果,以及后续等差线的计算结果。

因此,后续分析主要针对本文方法和十步相移法。

将图 4(d)和(g)的等倾线数据去包裹处理,得到实验结果如图 5 所示。显然,两种方法得到去包裹后的等倾线图像仍然具有一致性。

表 8 是在载荷 200 N、250 N、300 N、350 N 和更换

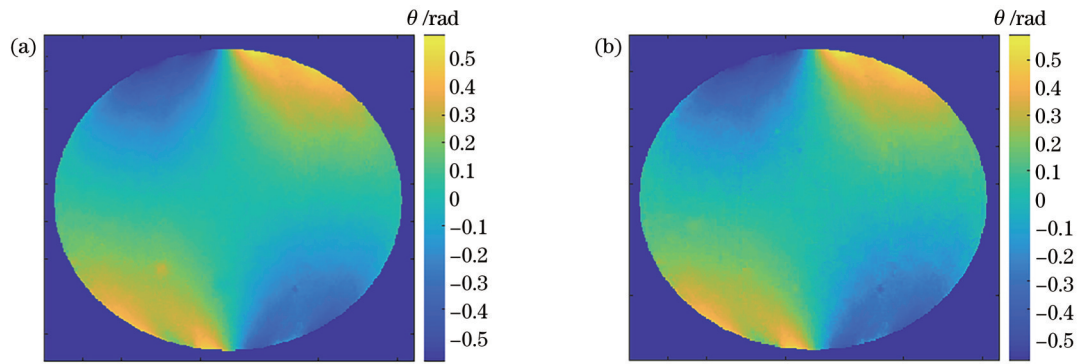


图 5 去包裹的等倾线图像。(a)十步相移;(b)本文的方法;
Fig. 5 Unwrapped isoclinic images. (a) Ten-step phase shift; (b) proposed method

圆盘材料尺寸条件下,本文方法和十步相移法计算得

表 8 等倾线和等差线的平均偏差结果

Table 8 Average deviation results of the isoclinic and isochromatic

Diameter D / mm	Loading F / N	Deviation of isoclinic B / rad	Deviation of isochromatic B / rad
50	200	0.0106	0.0802
50	250	0.0086	0.0934
50	300	0.0099	0.0926
50	350	0.0117	0.0960
40	200	0.0090	0.0919

到等倾线和等差线相位图的平均偏差结果。可见,实验减少了一张图像,等倾线平均偏差都稳定在 0.01 rad。

由此可以得出结论,本文方法与六步相移法相比,解决了等倾线受到等差线噪声干扰、出现不连续的锯齿缺陷的问题,去包裹等倾线相位更稳定。相比于十步相移法,本文方法在保持计算精度的前提下减少了需采集图像数量。

4.4 等差线实验结果分析

图 6 是载荷 $F=200$ N、 $D=50$ mm 下的等差线包裹相位图。图 7 是在图 6 的水平位置 1 和与水平夹角 30° 的 2 处,两种方法的等差线偏差曲线图。

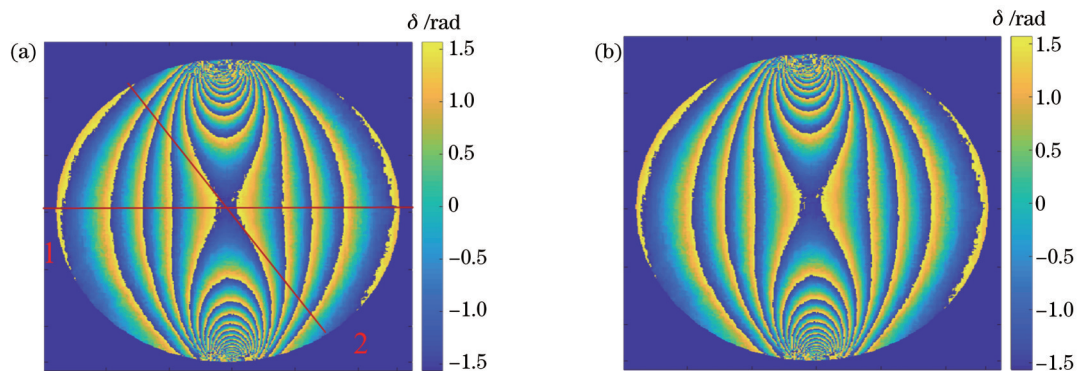


图 6 等差线图像。(a)十步相移;(b)本文的方法
Fig. 6 Isochromatic images. (a) Ten-step phase shift; (b) proposed method

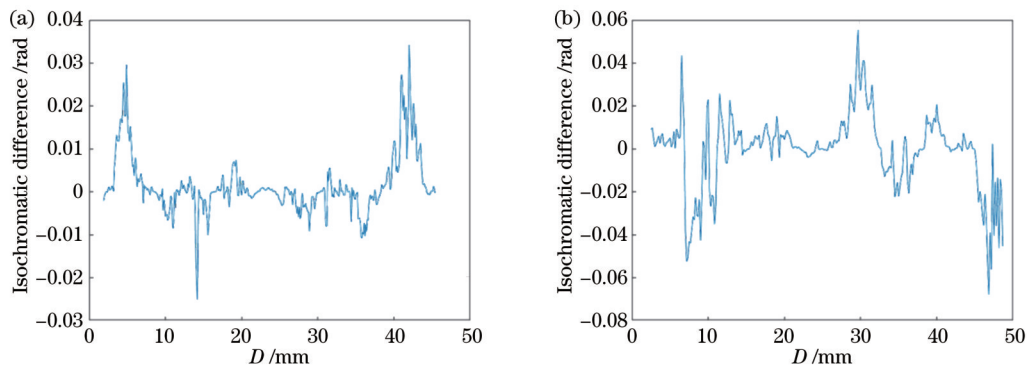


图 7 等差线偏差的曲线图。(a)圆盘位置 1 处;(b)圆盘位置 2 处
Fig. 7 Plot of isochromatic difference. (a) Location 1 of disc; (b) location 2 of disc

由图 6 可知,本文方法与十步相移法得到的等差线包裹相位图形状一致。为了进一步验证,通过图 7 的偏差曲线图可以看出,位置 1 和 2 的等差线都比较接近。

在改变载荷大小 F 、圆盘直径 D 等条件下,重复实验的结果如图 8 所示,对应的等差线平均偏差如表 8

所示。

图 8(a)(d)和(b)(e)是不同载荷下对比,图 8(c)(f)与图 5 是不同圆盘直径下对比,等差线图像形状都具有有一致性。根据表 8 中等差线偏差数值分析可知,偏差约为 0.09 rad。

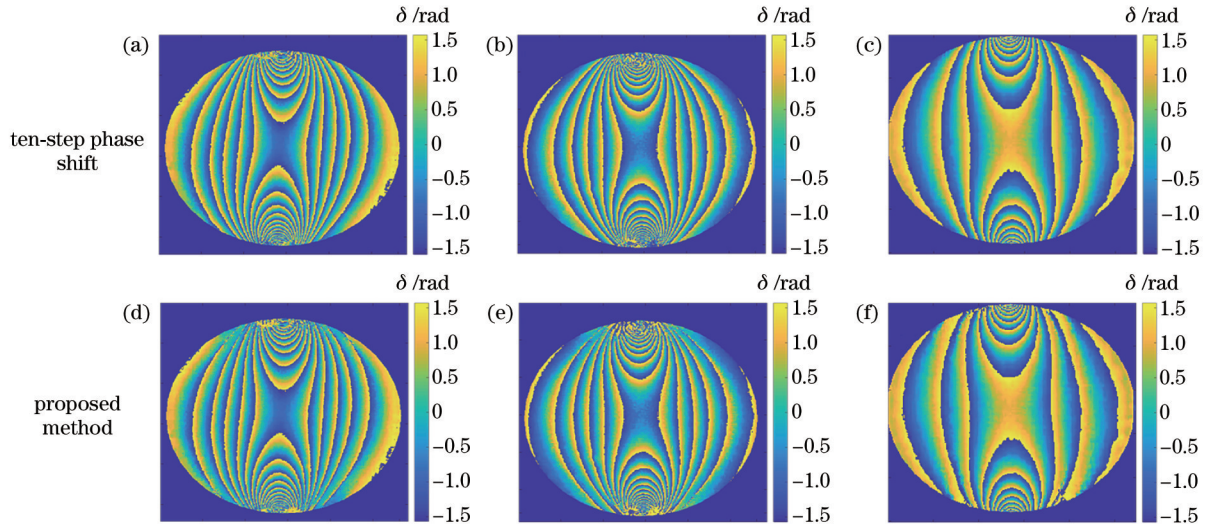


图 8 包裹的等差线图像。(a)(d) $F=300\text{ N}$, $D=50\text{ mm}$; (b)(e) $F=350\text{ N}$, $D=50\text{ mm}$; (c)(f) $F=200\text{ N}$, $D=40\text{ mm}$
Fig. 8 Wrapped isochromatic images. (a)(d) $F=300\text{ N}$, $D=50\text{ mm}$; (b)(e) $F=350\text{ N}$, $D=50\text{ mm}$; (c)(f) $F=200\text{ N}$, $D=40\text{ mm}$

5 结 论

本文分析了六步和十步相移法各自的缺点,提出了一种优化的混合相移方法,即用白光入射平面偏振光场的三幅光弹图像以及单色光入射圆偏振光场的三幅光弹图像分别计算等倾线和等差线,平衡了六步和十步相移的效率和精度。通过仿真模拟实验,验证了本文方法具有良好的抗噪性和相移误差抗干扰能力。对径向压缩的聚碳酸酯圆盘实验结果表明:本文方法可实现计算等倾线和等差线;与传统的六步相移法相比,本文方法避免了等倾线受到等差线干扰出现不连续的锯齿形缺陷;与十步相移法相比,两种方法计算的等倾线和等差线图像特征一致,等倾线的平均偏差在 0.01 rad,等差线的平均偏差在 0.09 rad,总体上减少了 4 幅图像数量,提高了 40% 采集效率。通过改变载荷、圆盘直径条件下的重复实验,验证了本文方法的有效性。

参 考 文 献

- [1] 刘志帆, 蔡燕民, 步扬, 等. 基于有限元分析方法的深紫外波段熔石英应力双折射分析[J]. 光学学报, 2021, 41(12): 1226001.
Liu Z F, Cai Y M, Bu Y, et al. Stress birefringence analysis in fused silica at deep ultraviolet waveband based on finite element simulation method[J]. Acta Optica Sinica, 2021, 41(12): 1226001.
- [2] 齐乃杰, 袁晓东, 张丽娟, 等. 激光损伤残余应力三维检测技术[J]. 中国激光, 2020, 47(10): 1004001.
- [3] Qi N J, Yuan X D, Zhang L J, et al. Three-dimensional detection technology of laser damage residual stress[J]. Chinese Journal of Lasers, 2020, 47(10): 1004001.
- [4] Ramesh K, Mangal S K. Data acquisition techniques in digital photoelasticity: a review[J]. Optics and Lasers in Engineering, 1998, 30(1): 53-75.
- [5] Ramesh K, Lewis G. Digital photoelasticity: advanced techniques and applications[J]. Applied Mechanics Reviews, 2002, 55(4): B69-B71.
- [6] Ju Y, Wang Y, Ren Z, et al. Optical method to quantify the evolution of whole-field stress in fractured coal subjected to uniaxial compressive loads[J]. Optics and Lasers in Engineering, 2020, 128: 106013.
- [7] Ren Z, Xie H, Ju Y. Determination of the stress and strain fields in porous structures by photoelasticity and digital image correlation techniques[J]. Polymer Testing, 2021, 102: 107315.
- [8] Brínez-de León J C, Restrepo-Martínez A, Branch-Bedoya J W. Computational analysis of Bayer colour filter arrays and demosaicking algorithms in digital photoelasticity[J]. Optics and Lasers in Engineering, 2019, 122: 195-208.
- [9] Guo E H, Liu Y G, Han Y S, et al. Full-field stress determination in photoelasticity with phase shifting technique[J]. Measurement Science and Technology, 2018, 29(4): 045208.
- [10] Patterson E A, Wang Z F. Towards full field automated photoelastic analysis of complex components[J]. Strain, 1991, 27(2): 49-53.
- [11] 钟振威, 贺玲凤. 改进的六步相移法确定等倾角与等差线相位 [J]. 实验力学, 2013, 28(4): 524-528.
Zhong Z W, He L F. On the determination of isoclinic angle and isochromatic line by a improved six-step phase shifting method [J]. Journal of Experimental Mechanics, 2013, 28(4): 524-528.
- [12] Gao Y, Wan X J, Xie S P, et al. Error analysis and correction equations for a real-time phase-shifting method using circular polariscope-based photoelasticity[J]. Optik, 2022, 265: 169528.
- [12] 万新军, 高阳, 韦晓孝, 等. 圆偏场瞬时光弹相移法的波长失

- 配误差及补偿[J]. 光学学报, 2022, 42(21): 2112002.
- Wan X J, Gao Y, Wei X X, et al. Wavelength mismatch error and compensation analysis of instantaneous photoelastic phase-shifting method in circularly polarized field[J]. Acta Optica Sinica, 2022, 42(21): 2112002.
- [13] Ajovalasit A, Barone S, Petrucci G. A method for reducing the influence of quarter-wave plate errors in phase stepping photoelasticity[J]. The Journal of Strain Analysis for Engineering Design, 1998, 33(3): 207-216.
- [14] Brown G M, Sullivan J L. The computer-aided holophotoelastic method[J]. Experimental Mechanics, 1990, 30(2): 135-144.
- [15] Petrucci G. Full-field automatic evaluation of an isoclinic parameter in white light[J]. Experimental Mechanics, 1997, 37(4): 420-426.
- [16] Zhenkun L, Dazhen Y, Wanming Y. Whole-field determination of isoclinic parameter by five-step color phase shifting and its error analysis[J]. Optics and Lasers in Engineering, 2003, 40(3): 189-200.
- [17] Ramji M, Gadre V Y, Ramesh K. Comparative study of evaluation of primary isoclinic data by various spatial domain methods in digital photoelasticity[J]. The Journal of Strain Analysis for Engineering Design, 2006, 41(5): 333-348.
- [18] Ramji M, Ramesh K. Whole field evaluation of stress components in digital photoelasticity: issues, implementation and application[J]. Optics and Lasers in Engineering, 2008, 46(3): 257-271.
- [19] Ramesh K, Sasikumar S. Digital photoelasticity: recent developments and diverse applications[J]. Optics and Lasers in Engineering, 2020, 135: 106186.
- [20] Xu Z K, Han Y S, Shao H L, et al. High-precision stress determination in photoelasticity[J]. Applied Mathematics and Mechanics, 2022, 43(4): 557-570.
- [21] Onuma T, Otani Y. A development of two-dimensional birefringence distribution measurement system with a sampling rate of 1.3 MHz[J]. Optics Communications, 2014, 315: 69-73.
- [22] Iwatsuki S, Hidai H, Chiba A, et al. Examination of internal stress by photoelasticity in laser cleaving of glass[J]. Precision Engineering, 2020, 64: 122-128.
- [23] Xu Z K, Zhang S Q, Han Y S, et al. Full-field phase shifting and stress quantification using a polarization camera[J]. Measurement, 2022, 201: 111727.

Six-Step Hybrid Phase Shift Technique in Digital Photoelasticity

Qiu Chuan¹, Chen Niannian¹, Wu Ling^{1*}, Fan Yong^{1**}, Liu Guanghai²

¹*School of Computer Science and Technology, Southwest University of Science and Technology, Mianyang 621010, Sichuan, China;*

²*Sichuan Physcience Optics and Fine Mechanics Co., Ltd., Mianyang 621010, Sichuan, China*

Abstract

Objective In digital photoelasticity, the stress field contains isoclinic information of the main stress direction angle and isochromatic information of the main stress difference, both of which are indispensable in stress calculation, so it is very important to obtain isoclinic and isochromatic information quickly and accurately. The ten-step phase shift method is the most widely used one, as it solves the problem of isoclinic and isochromatic line coupling in the six-step phase shift method for monochromatic light. Although the ten-step phase shift method has higher measurement accuracy, its efficiency is lower due to the acquisition of four white light incident images. Some researchers have improved the image acquisition devices, such as expensive polarization sensors, to increase efficiency. This paper proposes a minimal phase shift scheme that satisfies the requirements of calculating an isoclinic line in a planar polarized light field and an isochromatic line in a circularly polarized light field, so as to balance measurement accuracy and efficiency.

Methods In photoelasticity experiments, the planar polarized light field with white light incidence has more advantages than the circularly polarized light field with monochromatic light incidence, and the isoclinic line calculated based on the former field effectively avoids the problem of coupling with isochromatic line. Therefore, in this paper, under the planar polarized light field with white light incidence, the isoclinic line is calculated by reducing photoelastic images from 4 to 3, which effectively avoids the problem of isoclinic and isochromatic line coupling and quarter wave plate mismatch errors. For the problem of low efficiency of the ten-step phase shift method caused by acquiring massive images, this paper reduces photoelastic images from 6 to 3, so as to calculate isochromatic line under the circularly polarized light field with monochromatic light incidence, which solves the problem of low efficiency due to image acquisition. In the next simulation experiment, this paper calculates the isoclinic and isochromatic lines under different noise levels to evaluate their anti-noise performance. In addition, the paper calculates isoclinic and isochromatic lines under different azimuth errors to evaluate the anti-jamming capability of phase shift errors. Furthermore, the effectiveness of the proposed method is verified by a radially compressed polycarbonate disc.

Results and Discussions Firstly, in view of the problem of isoclinic and isochromatic line coupling caused by monochromatic light in the traditional six-step phase shift method and the low data acquisition efficiency in the ten-step

phase shift method, a six-step hybrid phase shift method is designed, which changes the 6+4 measurement method in the ten-step phase shift method to 3+3 measurement method. The feasibility of this method is verified by real experimental data. In addition, compared with the traditional six-step phase shift method, the six-step hybrid phase shift method effectively avoids the problems of isoclinic and isochromatic line coupling and quarter wave plate mismatch errors (Fig. 4); compared with the ten-step phase shift method, the method has an average deviation of isoclinic line of about 0.01 rad and an average deviation of isochromatic line of about 0.09 rad (Table 8). Furthermore, the proposed method reduces image quantity and improves the acquisition efficiency by 40% while ensuring measurement accuracy (Fig. 5–Fig. 8). Secondly, in order to verify the noise immunity and phase shift error immunity of the six-step hybrid phase shift method, the deviations of isoclinic and isochromatic lines calculated under different noise levels are generally comparable to those of the ten-step phase shift method (Table 5), and the deviations of isoclinic line calculated under different azimuth errors are consistent with those of the ten-step phase shift method, which indicates that this method has the same immunity to phase shift error interference as the ten-step phase shift method (Table 6). The deviations of the isochromatic line calculated under different azimuth errors are approximately twice as large as those of the ten-step phase shift method (Table 7). The reason for this is that the ten-step phase shift method uses six images to calculate the isochromatic line, while the proposed method only requires three images, but it loses some effective information to a certain extent, so the resistance to phase error interference of the proposed method is relatively weak compared with that of the ten-step phase shift method.

Conclusions This paper analyzes the disadvantages of the six-step and ten-step phase shift methods and proposes an optimized six-step hybrid phase shift method. The paper uses three photoelastic images of a planar polarized light field with white light incidence and three photoelastic images of a circularly polarized light field with monochromatic light incidence to calculate isoclinic and isochromatic lines separately and balance the efficiency and accuracy of the six-step and ten-step phase shift methods. Through the simulation experiment of the radially compressed disc, it is verified that the proposed method has excellent anti-noise and anti-interference abilities for phase shift errors. The experimental results of the radially compressed polycarbonate discs show that compared with the traditional six-step phase shift method, the proposed method avoids the problem of isoclinic and isochromatic coupling. Furthermore, the features of the isoclinic and isochromatic images calculated by the proposed method are consistent with those calculated by the ten-step phase shift method. The average deviation of the isoclinic line is 0.01 rad, and the average deviation of the isochromatic line is 0.09 rad. The proposed method reduces the number of images, and the acquisition efficiency is improved by 40%. The effectiveness of this method is verified by repeated experiments under the conditions of changing load and disc diameter.

Key words physical optics; digital photoelasticity; phase shift method; isoclinic line; isochromatic line